

# The redshift evolution of escape fraction of hydrogen ionizing photons from galaxies

Vikram Khaire<sup>1</sup> <sup>\*</sup>, Raghunathan Srianand<sup>1</sup>, Tirthankar Roy Choudhury<sup>2</sup>,  
and Prakash Gaikwad<sup>2</sup>

<sup>1</sup>*Inter-University Centre for Astronomy and Astrophysics (IUCAA), Post Bag 4, Pune 411007, India*

<sup>2</sup>*National Centre for Radio Astrophysics, Tata Institute of Fundamental Research, Pune 411007, India*

Accepted 2016 January 20.

## ABSTRACT

Using our cosmological radiative transfer code, we study the implications of the updated quasi-stellar object (QSO) emissivity and star formation history for the escape fraction ( $f_{\text{esc}}$ ) of hydrogen ionizing photons from galaxies. We estimate the  $f_{\text{esc}}$  that is required to reionize the Universe and to maintain the ionization state of the intergalactic medium in the post-reionization era. At  $z > 5.5$ , we show that a constant  $f_{\text{esc}}$  of 0.14 to 0.22 is sufficient to reionize the Universe. At  $z < 3.5$ , consistent with various observations, we find that  $f_{\text{esc}}$  can have values from 0 to 0.05. However, a steep rise in  $f_{\text{esc}}$ , of at least a factor of  $\sim 3$ , is required between  $z = 3.5$  to 5.5. It results from a rapidly decreasing QSO emissivity at  $z > 3$  together with a nearly constant measured H I photoionization rates at  $3 < z < 5$ . We show that this requirement of a steep rise in  $f_{\text{esc}}$  over a very short time can be relaxed if we consider the contribution from a recently found large number density of faint QSOs at  $z \geq 4$ . In addition, a simple extrapolation of the contribution of such QSOs to high- $z$  suggests that QSOs alone can reionize the Universe. This implies, at  $z > 3.5$ , that either the properties of galaxies should evolve rapidly to increase the  $f_{\text{esc}}$  or most of the low-mass galaxies should host massive black holes and sustain accretion over a prolonged period. These results motivate a careful investigation of theoretical predictions of these alternate scenarios that can be distinguished using future observations. Moreover, it is also very important to revisit the measurements of H I photoionization rates that are crucial to the analysis presented here.

**Key words:** Cosmology: diffuse radiation – galaxies: evolution – quasars: general – galaxies: intergalactic medium

## 1 INTRODUCTION

The hydrogen in the intergalactic medium (IGM) is highly ionized at  $z < 6$  as shown by various observations of Lyman- $\alpha$  forest in high-redshift quasi-stellar object (QSO) spectra (Fan et al. 2006; Bolton et al. 2011; Goto et al. 2011) and the cosmic microwave background (CMB) polarization measurements (Larson et al. 2011). Prior to that the IGM went through a phase transition from a completely neutral to a highly ionized state through the process of H I reionization. In the most typical scenario, QSOs and the H I ionizing photons generated by the star-forming galaxies reionize the Universe and maintain the observed high ionization state of the IGM even after the epoch of reionization. However,

the relative contribution of galaxies to the total budget of H I ionizing photons is highly uncertain. This is because the fraction ( $f_{\text{esc}}$ ) of H I ionizing photons generated by stellar population inside the galaxies that escapes out into the IGM is ill-constrained.

Over the past decade, various observational studies have reported the average  $f_{\text{esc}}$  ranging from 0.02 to 0.5 at  $z \sim 3$  (Steidel et al. 2001; Shapley et al. 2006; Iwata et al. 2009; Boutsia et al. 2011; Nestor et al. 2013; Micheva et al. 2015). The recent deep observations of galaxies have demonstrated that most of the previously reported detections of the escaping H I ionizing photons are spurious due to contaminations from the low- $z$  intervening galaxies (Mostardi et al. 2015; Siana et al. 2015). The average  $f_{\text{esc}}$  inferred from a sample of galaxies are dominated by a handful of galaxies with high  $f_{\text{esc}}$ . At low- $z$ , apart from few individual galaxies with

\* E-mail: vikramk@iucaa.in

high  $f_{\text{esc}}$  (see for e.g. [Borthakur et al. 2014](#)), various observational studies found that a very small fraction of the H I ionizing photons do escape from galaxies and the derived upper limits on the average  $f_{\text{esc}}$  hardly exceed 0.05 ([Cowie et al. 2009](#); [Grimes et al. 2009](#); [Bridge et al. 2010](#); [Barger et al. 2013](#); [Leitet et al. 2013](#)).

On the other hand, theoretical studies have suggested a wide range of  $f_{\text{esc}}$  from 0.01 to 1 ([Dove & Shull 1994](#); [Ricotti & Shull 2000](#); [Gnedin et al. 2008](#); [Kimm & Cen 2014](#); [Roy et al. 2015](#)). There are various factors that influence the escape of H I ionizing photons such as the galaxy mass, morphology, supernova rates, composition of interstellar medium and the gas distribution ([Fernandez & Shull 2011](#); [Benson et al. 2013](#); [Kim et al. 2013](#); [Cen & Kimm 2015](#)). In a standard picture where population of bright QSOs decline rapidly at  $z > 3$ , one requires the contribution from galaxies to dominate the H I ionizing photon budget and drive the H I reionization. Observations related to H I reionization, such as galaxy luminosity functions at high redshift ([Bouwens et al. 2012](#); [Finkelstein et al. 2015](#)), hydrogen photoionization rates inferred from the Lyman- $\alpha$  forest seen in the QSO absorption spectra, and constraints on the electron scattering optical depth ( $\tau_{\text{el}}$ ) from CMB (e.g. from Wilkinson Microwave Anisotropy Probe; WMAP [Hinshaw et al. 2013](#)) have been used for constraining the  $f_{\text{esc}}$  at  $z > 6$ . An evolving  $f_{\text{esc}}$  at high- $z$  was necessary to match the WMAP  $\tau_{\text{el}} = 0.089 \pm 0.014$  ([Haardt & Madau 2012](#); [Kuhlen & Faucher-Giguère 2012](#); [Shull et al. 2012](#); [Mitra et al. 2013](#)) however, no such evolution is required to explain the recent  $\tau_{\text{el}} = 0.066 \pm 0.016$  from [Planck Collaboration et al. \(2015\)](#). Recently, [Mitra et al. \(2015\)](#) have carried out a Markov chain Monte Carlo based statistical analysis using a semi-analytical model of reionization to infer that the current data sets can be explained by a constant  $f_{\text{esc}} \sim 0.15$  at  $z > 6$ , though the uncertainties on the constraints are still high. [Bouwens et al. \(2015a\)](#) also find similar constraints on  $f_{\text{esc}}$  by computing the evolution of the ionizing emissivity from the galaxy luminosity functions.

The  $f_{\text{esc}}$  controls the ionizing emissivity of galaxies which is crucial to understand the H I reionization, thermal history of the IGM, and the ratio of column densities of He II to H I inferred in the IGM ([Khaire & Srianand 2013](#)). The  $f_{\text{esc}}$  is also important to study the implications of the trapped radiation in galaxies to understand the detectability of Lyman- $\alpha$  emission from primordial galaxies ([Tumlinson et al. 2001](#); [Rhoads et al. 2004](#)).

In this paper, we study the effect of updated QSO emissivity and star formation rate density (SFRD) on the required mean  $f_{\text{esc}}$  to keep the IGM ionized at the level required by different observations. We use the QSO emissivity from [Khaire & Srianand \(2015a\)](#) (hereafter, [KS15a](#)) which is obtained from a compilation of recent QSO luminosity functions (QLFs). We use a self-consistently calculated SFRD along with the dust attenuation from [Khaire & Srianand \(2015b\)](#) (hereafter, [KS15b](#)) obtained by compiling various multi-wavelength and multi-epoch galaxy luminosity functions. To constrain  $f_{\text{esc}}$  in the post-reionization era ( $z \lesssim 6$ ), we use the measured H I photoionization rates ([Bolton & Haehnelt 2007](#); [Calverley et al. 2011](#); [Wytke & Bolton 2011](#); [Becker & Bolton 2013](#); [Kollmeier et al. 2014](#); [Shull et al. 2015](#)) and in the pre-

reionization era ( $z \gtrsim 6$ ), we calculate reionization histories consistent with the  $\tau_{\text{el}}$  constraints from Planck along with the recent mean H I fraction measurements ([Schenker et al. 2014](#); [McGreer et al. 2015](#)). We calculate the H I ionizing UV background (UVB; in this paper it implies a background radiation at  $\lambda < 912 \text{ \AA}$ ) using a radiative transfer code developed by us ([Khaire & Srianand 2013](#)) following the standard prescription ([Miralda-Escude & Ostriker 1990](#); [Shapiro et al. 1994](#); [Haardt & Madau 1996](#); [Fardal et al. 1998](#); [Shull et al. 1999](#); [Faucher-Giguère et al. 2009](#)) albeit keeping  $f_{\text{esc}}$  as a free parameter. Then, we constrain  $f_{\text{esc}}(z)$  by comparing the model predictions with the observations mentioned above. We also study the implications of high QSO emissivity at  $z > 4$  obtained using the recent QLFs reported by [Giallongo et al. \(2015\)](#) on the  $f_{\text{esc}}$  and H I reionization.

The plan of the paper is as follows. In Section 2, we present the basic theory to evaluate the UVB in pre- and post-reionization era. We review the form of H I ionizing emissivity from QSOs and galaxies used in our models in Section 3. In Section 4, we summarize the constraints on  $f_{\text{esc}}$  in the post- and pre-reionization era for different possible QSO emissivities as a function of  $z$ . We also explore an extreme case where all the H I ionizing photons required for the reionization are sourced by QSOs alone (i.e. with  $f_{\text{esc}} = 0$ ). In Section 5, we summarize the results. Throughout this paper we use a flat  $\Lambda$ CDM cosmology with  $\Omega_{\Lambda} = 0.7$ ,  $\Omega_m = 0.3$  and  $H_0 = 70 \text{ km s}^{-1} \text{ Mpc}^{-1}$ .

## 2 BASIC THEORY

The definition of escape fraction ( $f_{\text{esc}}$ ) of H I ionizing photons from galaxies used in this paper is

$$f_{\text{esc}} = \frac{L(912\text{\AA})_{\text{esc}}}{L(912\text{\AA})_{\text{int}}}, \quad (1)$$

where,  $L(912\text{\AA})_{\text{esc}}$  and  $L(912\text{\AA})_{\text{int}}$  are the escaping and intrinsic specific luminosities at  $\lambda = 912 \text{ \AA}$ , respectively. The procedure we use to estimate the mean  $f_{\text{esc}}$  from galaxies at all epochs is briefly described here. We estimate the mean specific intensity  $J_{\nu}(z)$  of the H I ionizing UVB (contributed by both QSOs and galaxies) by taking  $f_{\text{esc}}(z)$  as a free parameter. Using this, we obtain H I photoionization rates ( $\Gamma_{\text{HI}}$ ), defined as

$$\Gamma_{\text{HI}}(z) = \int_{\nu_{912}}^{\infty} \frac{4\pi J_{\nu}(z) \sigma_{\text{HI}}(\nu) d\nu}{h\nu}, \quad (2)$$

where  $\nu_{912}$  is the frequency of photons having energy equal to the ionization potential of H I (13.6 eV or 912  $\text{\AA}$ ),  $\sigma_{\text{HI}}(\nu)$  is the H I photoionization cross-section and  $h$  is the Planck constant. To constrain  $f_{\text{esc}}(z)$ , in the post-reionization era, we compare predicted  $\Gamma_{\text{HI}}(z)$  from our models with its measurements (see [Inoue et al. 2006](#), for a similar method) and in the pre-reionization era, we compare our model predictions with the recent constraints on  $\tau_{\text{el}}$  from Planck and the mean fraction of H I.

The method described above depends crucially on the the H I ionizing UVB. The UVB at any point in the Universe is the mean intensity of UV radiation arriving at that point generated by the relevant sources and filtered through gas in the IGM. Therefore, apart from the ionizing emissivity

of the radiating sources, the distribution of gas in the IGM is also essential for computing the UVB. In this section, we provide the basic theory required to estimate the UVB and describe the models used for the IGM gas distribution in both pre- and post-reionization era.

## 2.1 UV background at all epochs

In the post-reionization era, the mean free path of H I ionizing photons is large enough to consider the UVB as essentially uniform. In the pre-reionization era, each source or the cluster of sources of the H I ionizing photons create a bubble of H II around them. The volume filling factor ( $Q_{\text{HII}}$ ) of all these H II bubbles, defined as the ratio of the volume occupied by all such H II bubbles to the total volume of the Universe, is crucial for understanding the dynamics of the H I reionization. The  $Q_{\text{HII}}$  is usually obtained under the assumption that the interior of all such H II bubbles have, on an average, a uniform UVB (however, see Meiksin & White 2003, for local fluctuations in the UVB). Therefore, in the pre-reionization era, the UVB is within the H II bubbles and there are no H I ionizing UV photons outside the bubbles (see Choudhury 2009). The  $Q_{\text{HII}}(z)$  is equal to unity in the post-reionization era and the exact value of it ( $Q_{\text{HII}}(z) < 1$ ) in the pre-reionization era depends on the model of the H I reionization. Taking all these into consideration, the mean specific intensity of UVB,  $J_{\nu_0}$  (in units of  $\text{erg cm}^{-2} \text{s}^{-1} \text{Hz}^{-1} \text{sr}^{-1}$ ), at all epochs  $z_0$  and frequency  $\nu_0$  can be evaluated by solving the following integral (see Peebles 1993; Haardt & Madau 1996),

$$J_{\nu_0}(z_0) = \frac{c}{4\pi} \int_{z_0}^{\infty} dz \frac{(1+z_0)^3 \epsilon_{\nu}(z)}{(1+z)H(z)Q_{\text{HII}}(z)} e^{-\tau_{\text{eff}}(\nu_0, z_0, z)}. \quad (3)$$

Here, the  $H(z) = H_0 \sqrt{\Omega_m(1+z)^3 + \Omega_{\Lambda}}$  is the Hubble parameter,  $c$  is the speed of light and  $\epsilon_{\nu}(z)$  is the comoving H I ionizing emissivity of the sources. The  $Q_{\text{HII}}(z)$  in the denominator makes our UVB different from the UVB model of Haardt & Madau (2012, hereafter, HM12) in the pre-reionization era. This ensures that the H I ionizing photons are confined within the H II bubbles in the pre-reionization era.<sup>1</sup> This approximation of uniform UVB within the H II bubbles breaks down at very small values of  $Q_{\text{HII}}$ . The  $\tau_{\text{eff}}(\nu_0, z_0, z)$  is an effective optical depth encountered by the ionizing photons while travelling from the emission redshift  $z > z_0$  with a frequency  $\nu > \nu_0$  to arrive at redshift  $z_0$  and frequency  $\nu_0$ . Therefore, the relation between  $\nu$  and  $\nu_0$  is given by  $\nu = \nu_0(1+z)/(1+z_0)$ .

For a Poisson distributed H I clouds in the IGM, the  $\tau_{\text{eff}}$  is given by (see Paresce et al. 1980; Padmanabhan 2002),

$$\tau_{\text{eff}}(\nu_0, z_0, z) = \int_{z_0}^z dz' \int_0^{\infty} dN_{\text{HI}} f(N_{\text{HI}}, z') (1 - e^{-\tau_{\nu'}}). \quad (4)$$

Here,  $f(N_{\text{HI}}, z') = \frac{d^2 N}{dN_{\text{HI}} dz'}$  is the number of H I clouds per unit redshift and column density interval  $N_{\text{HI}}$  to  $N_{\text{HI}} + dN_{\text{HI}}$ . The continuum optical depth  $\tau_{\nu'}$  is

$$\tau_{\nu'} = N_{\text{HI}} \sigma_{\text{HI}}(\nu') + N_{\text{HeI}} \sigma_{\text{HeI}}(\nu') + N_{\text{HeII}} \sigma_{\text{HeII}}(\nu'), \quad (5)$$

where,  $\nu' = \nu_0(1+z)/(1+z_0)$ , and  $N_i$  and  $\sigma_i$  are the column density and photoionization cross-section, respectively, for species  $i$ . The ionization potential of He I (24.6 eV) is close to that of H I, and total helium is an order of magnitude less abundant by number compare to hydrogen. Therefore, the contribution of He I to the continuum optical depth is negligible. We do not consider this term (second term in Eq. 5) further in our analysis.

In the post-reionization era, to calculate  $\tau_{\text{eff}}$  we use the  $f(N_{\text{HI}}, z)$  given by Inoue et al. (2014). It is consistent with the various measurements of the H I column density distributions from Lyman- $\alpha$  forest (Kim et al. 2013), Lyman limit systems (Prochaska et al. 2014; O'Meara et al. 2013, 2007) and damped Lyman- $\alpha$  systems (Noterdaeme et al. 2009, 2012), the mean free path of H I ionizing photons (Worseck et al. 2014b) and the opacity of the IGM to Lyman- $\alpha$  photons (Fan et al. 2006; Becker et al. 2013). To calculate the UVB at wavelength  $\lambda < 228 \text{ \AA}$ , we follow the prescription given in HM12 to obtain the ratio of  $N_{\text{HeII}}$  to  $N_{\text{HI}}$ .

In the pre-reionization era, the helium within the H II bubbles created by galaxies is mostly in He II. Consequently, the UVB at  $\lambda < 228 \text{ \AA}$  is negligible owing to its photo-absorption by He II. This may not be true for the H II bubbles created by bright QSOs. However, this wavelength range ( $\lambda < 228 \text{ \AA}$ ) has negligible effect on the  $\Gamma_{\text{HI}}$  because of the  $\nu^{-3}$  dependence of the  $\sigma_{\text{HI}}(\nu)$ . Therefore, in the pre-reionization era, we simplify the Eq. (5) to  $\tau_{\nu'} = N_{\text{HI}} \sigma_{\text{HI}}(\nu')$  and estimate the UVB at  $\lambda > 228 \text{ \AA}$ . However, we still need the  $f(N_{\text{HI}}, z)$  that can not be directly measured due to large Gunn-Peterson optical depths at high- $z$ . We obtain  $f(N_{\text{HI}}, z)$  by using a large number of random lines of sight generated through a high-resolution hydrodynamical simulation box as explained in the following section.

## 2.2 $f(N_{\text{HI}}, z)$ within H II bubble

We use a high-resolution hydrodynamic P-GADGET3 simulation<sup>2</sup> (Springel 2005) with  $2 \times 512^3$  particles and a box size of  $10 h^{-1} \text{ cMpc}$  to study the hydrogen distribution and to obtain the  $f(N_{\text{HI}}, z)$ . These boxes are generated from  $z = 9$  to 5 with redshift interval of 0.5. In each box a large number of random lines of sight (LOS) were drawn. We use these LOS to probe the hydrogen distribution at different  $z$ .

For a given  $\Gamma_{\text{HI}}$  in the simulation box, one can calculate the H I and H II fraction assuming the photoionization equilibrium. However, to model the optically thin and thick absorption systems together, we need to consider the values of the local rate,  $\Gamma_{\text{HI}}^{\text{local}}$ , in regions with a range of overdensities. We use an empirical fit to the radiative transfer prescription of Rahmati et al. (2013), with a slight modification by Choudhury et al. (2015):

$$\frac{\Gamma_{\text{HI}}^{\text{local}}}{\Gamma_{\text{HI}}} = 0.98 \left[ 1 + \left( \frac{\Delta_{\text{H}}}{\Delta_{\text{ss}}} \right)^{1.64} \right]^{-2.28} + 0.02 \left[ 1 + \frac{\Delta_{\text{H}}}{\Delta_{\text{ss}}} \right]^{-0.84}, \quad (6)$$

where,  $\Delta_{\text{H}}$  is the overdensity of hydrogen and  $\Delta_{\text{ss}}$  is the threshold density.  $\Delta_{\text{ss}}$  is calculated assuming that the size

<sup>1</sup> Note that, the  $Q_{\text{HII}}(z)$  in the denominator can give rise to very high values of  $J_{\nu}(z)$  and  $\Gamma_{\text{HI}}(z)$  when it is very small.

<sup>2</sup> The simulation uses  $\sigma_8 = 0.827$ ,  $n_s = 0.96$  and  $\Omega_b = 0.048$ .

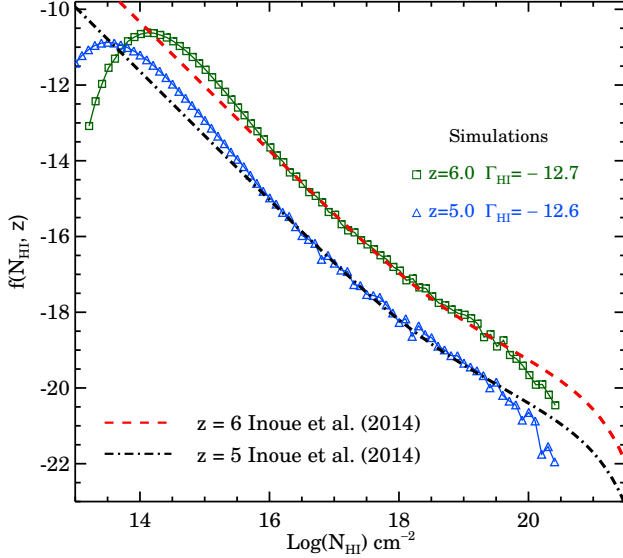


**Figure 1.** The  $f(N_{\text{HI}}, z)$  at  $z = 5$  (blue triangles) and  $z = 6$  (green squares) obtained from the simulations using the method outlined in Section 2.2 are shown along with the fits obtained by Inoue et al. (2014) (black and red curves) using various observations. The  $f(N_{\text{HI}}, z)$  at  $z = 6$  is scaled up by factor 10 for the clarity in presentation. Over the relevant column density range for evaluating  $\tau_{\text{eff}}$  i.e.,  $19.5 > \log N_{\text{HI}} > 15.5$ , the  $f(N_{\text{HI}}, z)$  matches quite well with the observations for the values of  $\Gamma_{\text{HI}}$  indicated in the plot. These  $\Gamma_{\text{HI}}$  values are chosen to be consistent with the measurements of Bolton & Haehnelt (2007), Calverley et al. (2011) and Wyithe & Bolton (2011).

of each absorber is given by the Jeans length (Schaye 2001),

$$\Delta_{\text{ss}} = 36 \left( \frac{\Gamma_{\text{HI}}}{10^{-12} \text{s}^{-1}} \right)^{2/3} \left( \frac{T}{10^4 \text{K}} \right)^{2/15} \left( \frac{\mu}{0.61} \right)^{1/3} \left( \frac{\chi}{1.08} \right)^{-2/3} \left( \frac{1+z}{8} \right)^{-3}, \quad (7)$$

where,  $T$  is the gas temperature,  $\chi$  is the number of electrons per H II ion in the H II bubble and  $\mu$  is the mean molecular weight. We take a constant  $T = 20000\text{K}$  for the gas temperature within each H II bubble. The value of  $\Delta_{\text{ss}}$  calculated in this way becomes unrealistically small for low  $\Gamma_{\text{HI}}$  at high  $z$ . Therefore, we impose a lower cut-off on  $\Delta_{\text{ss}} \geq 2$  (see Bolton & Haehnelt 2013).

Using this prescription, we calculate the H I column density of the absorbers along each line of sight by integrating the  $n_{\text{HI}}$  over a characteristic Jeans length ( $L_{\text{ss}}$ ) which is given by (Bolton & Haehnelt 2013)

$$L_{\text{ss}} = 8.7 \text{pkpc} \left( \frac{\Gamma_{\text{HI}}}{10^{-12} \text{s}^{-1}} \right)^{-1/3} \left( \frac{T}{10^4 \text{K}} \right)^{13/30} \left( \frac{\mu}{0.61} \right)^{-2/3} \left( \frac{\chi}{1.08} \right)^{1/3}. \quad (8)$$

It can have values between 20 to 40 pkpc in the redshift range of our interest ( $z > 5.5$ ). We follow Bolton & Haehnelt (2013) and use  $L_{\text{ss}} = 20$  pkpc throughout to estimate the  $f(N_{\text{HI}}, z)$ . For illustration, in Fig. 1, we show the  $f(N_{\text{HI}}, z)$  obtained in this way at two redshifts  $z = 5$

and 6 for  $\log(\Gamma_{\text{HI}} \text{s}^{-1}) = -12.6$  and  $-12.7$ , respectively. These  $\Gamma_{\text{HI}}$  values are consistent with the measurements at corresponding  $z$  (Bolton & Haehnelt 2007; Calverley et al. 2011; Wyithe & Bolton 2011). We also show the empirical fits to the  $f(N_{\text{HI}}, z)$  given by Inoue et al. (2014). At these redshifts, they match quite well with our estimates for  $19.5 > \log(N_{\text{HI}}) > 15.5$ . The  $\tau_{\text{eff}}$  is mostly dominated by this  $N_{\text{HI}}$  range. In the pre-reionization era, we use the  $f(N_{\text{HI}}, z)$  obtained from the simulations as explained above to estimate the UVB within the H II bubbles.

In the following section, we discuss the basic theory to obtain the  $Q_{\text{HII}}(z)$  in the pre-reionization era.

### 2.3 H II volume filling factor

Under the assumption of the photoionization equilibrium within a H II bubble, the time evolution of  $Q_{\text{HII}}$  can be written as (Madau et al. 1999; Barkana & Loeb 2001),

$$\frac{dQ_{\text{HII}}}{dt} = \frac{\dot{n}(t)}{\langle n_{\text{H}} \rangle} - \frac{\alpha_{\text{B}} \chi C \langle n_{\text{H}} \rangle Q_{\text{HII}}}{a^3(t)}. \quad (9)$$

Here,  $\dot{n}(t)$  is the comoving number density of H I ionizing photons per unit time,  $\langle n_{\text{H}} \rangle = 1.87 \times 10^{-7} \text{cm}^{-3}$  is the comoving number density of the total hydrogen,  $C$  is the clumping factor inside the H II bubbles,  $a(t)$  is the scale factor and  $\alpha_{\text{B}}$  is the case B recombination coefficient of hydrogen. In Eq. (9), the clumping factor is defined as  $C = \langle n_{\text{HII}}^2 \rangle / \langle n_{\text{H}} \rangle^2$  where  $n_{\text{HII}}$  is the number density of H II. The solution to the Eq. (9),  $Q_{\text{HII}}$ , at any redshift  $z_0$  is given by,

$$Q_{\text{HII}}(z_0) = \frac{1}{\langle n_{\text{H}} \rangle} \int_{z_0}^{\infty} \frac{\dot{n}(z)}{(1+z)H(z)} \exp \left[ -\alpha_{\text{B}} \langle n_{\text{H}} \rangle \times \int_{z_0}^z dz' \frac{\chi(z') C(z') (1+z')^2}{H(z')} \right] dz. \quad (10)$$

The reionization is completed when  $Q_{\text{HII}}(z_{\text{re}})$  becomes unity and the redshift  $z_{\text{re}}$  is called as the redshift of reionization.

We need the quantities  $\dot{n}(z)$  and  $C(z)$  to evaluate the evolution of  $Q_{\text{HII}}(z)$ . Note that the contribution to  $C(z)$  comes only from the ionized regions, and hence it is important to estimate the distribution of the self-shielded regions. This implies that  $C(z)$  depends on  $\Gamma_{\text{HI}}(z)$ . In fact, it is straightforward to obtain  $C$  from simulation boxes for an assumed value of  $\Gamma_{\text{HI}}$ . As described earlier,  $\Gamma_{\text{HI}}(z)$  depends on  $f(N_{\text{HI}}, z)$  and the comoving emissivity  $\epsilon_{\nu}(z)$ , which in turn determines the  $\dot{n}(z)$  through the relation

$$\dot{n}(z) = \int_{\nu_{912}}^{\infty} \frac{\epsilon_{\nu}(z) d\nu}{h\nu}. \quad (11)$$

Therefore, the values of  $\dot{n}(z)$  and  $C(z)$  cannot be chosen independently, they are rather related to each other through  $\Gamma_{\text{HI}}$  (or equivalently on  $\epsilon_{\nu}$ ). In this paper, we obtain the  $Q_{\text{HII}}$  for a given  $\epsilon_{\nu}(z)$  by self-consistently estimating the three quantities  $\dot{n}(z)$ , the UVB within H II bubbles and  $C(z)$ .

The  $\epsilon_{\nu}(z)$  has  $f_{\text{esc}}$  as a free parameter that we constrain using measurements of mean H I fraction and the  $\tau_{\text{el}}$  from Planck. Using the model predictions of  $Q_{\text{HII}}(z)$ , the  $\tau_{\text{el}}$  is given by

$$\tau_{\text{el}}(z) = c \langle n_{\text{H}} \rangle \sigma_{\text{T}} \int_0^z \chi(z') Q_{\text{HII}}(z') \frac{(1+z')^2}{H(z')} dz', \quad (12)$$

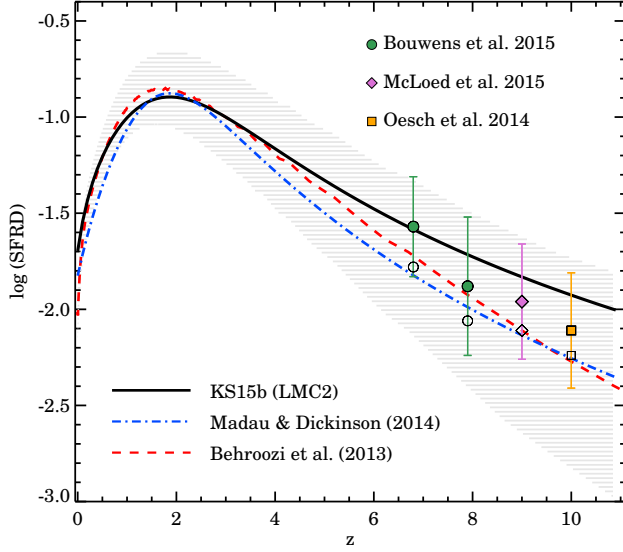


**Figure 2.** The SFRD( $z$ ) in units  $M_{\odot} \text{ yr}^{-1} \text{ Mpc}^{-3}$  from KS15b is shown along with the SFRD( $z$ ) obtained by Madau & Dickinson (2014) and by Behroozi et al. (2013), hatched gray region shows 1- $\sigma$  range) scaled to match the Salpeter IMF. The data points are the SFRD( $z$ ) calculated using the respective luminosity functions down to  $L_{\text{min}} = 0.01L^*$ . Empty symbols are obtained with no dust corrections and filled symbols are obtained using the dust corrections from KS15b. See text for more details.

where,  $\sigma_{\text{T}}$  is the Thompson electron scattering cross-section. We take  $\chi(z) = 1.16$  for  $z < 4$  where helium is assumed to be predominantly in He III and  $\chi(z) = 1.08$  for  $z > 4$  where helium is mostly in He II.

In the following section, we review the comoving H I ionizing emissivity  $\epsilon_{\nu}(z)$  from different sources used in our models.

### 3 IONIZING EMISSIVITY

The ionizing emissivity is estimated by considering the sources of H I ionizing photons ( $\lambda \leq 912 \text{ \AA}$ ) are only QSOs and star-forming galaxies. Therefore, the total comoving emissivity,  $\epsilon_{\nu}(z)$ , is the sum of the comoving QSO emissivity,  $\epsilon_{\nu}^{\text{Q}}(z)$ , and the comoving galaxy emissivity,  $\epsilon_{\nu}^{\text{G}}(z)$ . For the power-law spectral energy distribution (SED; for  $\lambda \leq 912 \text{ \AA}$ ) it can be written as,

$$\epsilon_{\nu}(z) = \left(\frac{\nu}{\nu_{912}}\right)^{\alpha} \epsilon_{\nu_{912}}^{\text{Q}}(z) + \left(\frac{\nu}{\nu_{912}}\right)^{\beta} \epsilon_{\nu_{912}}^{\text{G}}(z). \quad (13)$$

Here,  $\epsilon_{\nu_{912}}^{\text{Q}}(z)$  and  $\epsilon_{\nu_{912}}^{\text{G}}(z)$  are emissivities at  $912 \text{ \AA}$ , and  $\alpha$  and  $\beta$  are the indices of power-law SEDs for QSOs and galaxies, respectively, as given below.

The  $\epsilon_{\nu_{912}}^{\text{Q}}(z)$  in units of  $\text{erg s}^{-1} \text{ Hz}^{-1} \text{ Mpc}^{-3}$  is taken from KS15a. It has been obtained by fitting various QLFs<sup>3</sup> (Schulze et al. 2009; Croom et al. 2009; Glikman et al. 2011; Masters et al. 2012; Ross et al. 2013; Palanque-Delabrouille et al. 2013; McGreer et al. 2013; Kashikawa et al. 2015) and integrating the contribution of

QSOs down to a luminosity of  $0.01L^*$ , where  $L^*$  is the characteristic break luminosity of a QLF. It is given by,

$$\epsilon_{\nu_{912}}^{\text{Q}}(z) = 10^{24.6} (1+z)^{5.9} \frac{\exp(-0.36z)}{\exp(2.2z) + 25.1}, \quad (14)$$

with the  $\alpha = -1.4$  for  $\lambda < 912 \text{ \AA}$  in Eq. (13) (Stevens et al. 2014). Later, in this paper we also use the  $\epsilon_{\nu_{912}}^{\text{Q}}(z)$  obtained using the QLFs by Giallongo et al. (2015) at  $z > 4$  to explore the models of H I reionization with only QSOs.

We use the  $\epsilon_{\nu_{912}}^{\text{G}}(z)$  from KS15b. In KS15b, for different extinction curves, we determine self-consistent combinations of star formation rate density, SFRD( $z$ ), and dust attenuation magnitudes,  $A_{\text{FUV}}(z)$ , at the far-ultraviolet (FUV) band (central  $\lambda = 1500 \text{ \AA}$ ) using various multi-wavelength and multi-epoch galaxy luminosity functions. We find that the combination of SFRD( $z$ ) and  $A_{\text{FUV}}(z)$  obtained for an average extinction curve ( $k_{\nu}$ ) of the Large Magellanic Cloud Supershell (LMC2; Gordon et al. 2003) reproduces various observations. We use the combination of SFRD( $z$ ) (in units  $M_{\odot} \text{ yr}^{-1} \text{ Mpc}^{-3}$ ) and  $A_{\text{FUV}}(z)$  (in magnitudes) obtained for the LMC2 extinction curve in KS15b that is given by,

$$\text{SFRD}(z) = \frac{a + bz}{1 + (z/c)^d}; \quad A_{\text{FUV}}(z) = \frac{a_0 + b_0 z}{1 + (z/c_0)^{d_0}}, \quad (15)$$

with  $a = 2.01 \times 10^{-2}$ ,  $b = 8.48 \times 10^{-2}$ ,  $c = 2.5$ ,  $d = 3.09$ ,  $a_0 = 1.42$ ,  $b_0 = 0.93$ ,  $c_0 = 2.08$  and  $d_0 = 2.2$ . We use these to compute the  $\epsilon_{\nu}^{\text{G}}(z)$  as,

$$\epsilon_{\nu}^{\text{G}}(z) = C_{\nu}(z) \int_z^{\infty} \frac{\text{SFRD}(z') l_{\nu}[t(z) - t(z'), Z] dz'}{(1+z')H(z')}, \quad (16)$$

with the dust correction  $C_{\nu}(z)$  at  $\lambda > 912 \text{ \AA}$ ,

$$C_{\nu}(z) = 10^{-0.4 A_{\text{FUV}}(z) \frac{k_{\nu}}{k_{\text{FUV}}}}. \quad (17)$$

For  $\lambda \leq 912 \text{ \AA}$ , we take  $C_{\nu}(z) = f_{\text{esc}}(z)$  assuming that the SED does not get modified by the dust at  $\lambda < 912 \text{ \AA}$ . This can be interpreted as if the H I ionizing photons escape through the holes in the galaxies (Fujita et al. 2003; Paardekooper et al. 2011) or generated by few unobscured sources or runaway stars (Gnedin et al. 2008; Conroy & Kratter 2012). The free parameter  $f_{\text{esc}}(z)$  is a luminosity weighted angle averaged escape fraction treated in the same way as given in HM12. For  $\lambda < 228 \text{ \AA}$ , we take  $C_{\nu}(z) = 0$  assuming that He II ionizing photons do not escape from galaxies. The  $l_{\nu}[t(z) - t(z'), Z]$  is the specific luminosity of a simple stellar population (in units of  $\text{erg s}^{-1} \text{ Hz}^{-1}$  per unit total mass of stars formed) at redshift  $z$  having the age of  $t_0 = t(z) - t(z')$  that went through an instantaneous burst of star formation at redshift  $z'$  with an average metallicity  $Z$ . We obtain this using a population synthesis code STARBURST99 (Leitherer et al. 1999) for a Salpeter (1955) initial mass function (IMF) and a constant metallicity of 0.4 times solar value ( $Z_{\odot}$ ) for simplicity (i.e.,  $Z = 0.008$ ). We direct readers to Section 8 of KS15b for discussions on the effect of using different model parameters of stellar population on the derived SFRD( $z$ ) and  $A_{\text{FUV}}(z)$ . We obtain a simple fit to  $\epsilon_{\nu}^{\text{G}}(z)$  at  $912 \text{ \AA}$  in units of  $\text{erg s}^{-1} \text{ Hz}^{-1} \text{ Mpc}^{-3}$  as

$$\epsilon_{\nu_{912}}^{\text{G}}(z) = f_{\text{esc}}(z) \times 10^{25} \frac{3.02 + 13.12z}{1 + (z/2.44)^{3.02}}. \quad (18)$$

At  $\lambda < 912 \text{ \AA}$ , we find that  $\beta = -1.8$  in Eq. (13) approximates the SED for the assumed stellar population model.

<sup>3</sup> See, Table 1 and Section 3.1 of KS15a.

We verify that this exponent reproduces the  $\Gamma_{\text{HI}}$  and  $\dot{n}$  generated by the intrinsic spectrum. Note that the exponent  $\beta$  can have slightly different value depending on the assumed metallicity and the IMF (see, [Becker & Bolton 2013](#)).

We use a fixed IMF and metallicity to estimate  $\epsilon_{\nu_{912}}^G(z)$ . However, using different IMF and metallicities can change the intrinsic ionizing emissivity (i.e.  $\epsilon_{\nu_{912}}^G/f_{\text{esc}}$ ) generated inside galaxies. We estimate the uncertainty in this emissivity, while consistently reproducing the same  $\epsilon_{\text{FUV}}(z)$  used to determine the SFRD( $z$ ), for different IMFs and metallicities. We find that, when we change metallicity from  $Z = 0.4Z_{\odot}$  to  $Z = 0.005Z_{\odot}$ , the change in the intrinsic ionizing emissivity is less than 7%. Instead of our fiducial Salpeter IMF, when we use the [Kroupa \(2001\)](#) IMF (with exponents 1.3 and 2.3 for mass ranges 0.1 to 0.5  $M_{\odot}$  and 0.5 to 100  $M_{\odot}$ , respectively), increase in the intrinsic ionizing emissivity is less than 13%. However, using top heavy IMFs or the rotation in stars ([Topping & Shull 2015](#)) the intrinsic ionizing emissivity can be increased significantly.

In Fig. 2, we show the SFRD( $z$ ) used here (from Eq. 15). For comparison, we also show the SFRD( $z$ ) obtained by [Madau & Dickinson \(2014\)](#) and [Behroozi et al. \(2013\)](#). The SFRD( $z$ ) from the latter is multiplied by 1.7 to match the result for the Salpeter IMF used in other estimates. At  $z > 7$ , our SFRD( $z$ ) is higher than the mean SFRD( $z$ ) given in these papers by 0.2 to 0.4 dex (see Fig. 2). This difference arises because of the differences in the applied dust correction and the minimum luminosity ( $L_{\text{min}}$ ) down to which the FUV luminosity functions are integrated. In Fig. 2, we show the SFRD obtained using the recent high- $z$  measurements of the luminosity functions ([Oesch et al. 2014](#); [Bouwens et al. 2015b](#); [McLeod et al. 2015](#)). These points are obtained using the same scaling relation used in [KS15b](#),  $\text{SFRD}(z) = 1.25 \times 10^{-28} \epsilon_{\text{FUV}}(z) 10^{0.4A_{\text{FUV}}(z)} M_{\odot} \text{yr}^{-1} \text{Mpc}^{-3}$ , where,  $\epsilon_{\text{FUV}}$  is the emissivity at FUV band obtained by integrating the FUV luminosity functions down to  $L_{\text{min}} = 0.01L^*$ . The SFRD( $z$ ) used here is consistent with these measurements and is within  $1 - \sigma$  range predicted by [Behroozi et al. \(2013\)](#) (see the hatched region in Fig. 2).

For simplicity, we neglect the diffuse emission processes owing to their negligible contribution to UVB such as the He II Lyman and Balmer continuum emission, He II Lyman- $\alpha$  line emission and He I Lyman continuum emission.

Using the  $\epsilon_{\nu}(z)$  explained here, we place constraints on  $f_{\text{esc}}(z)$  at different epochs as discussed in the following section. The resulting trend in  $f_{\text{esc}}(z)$  prompted us to speculate on different QSO emissivities at  $z > 3.5$  which are also presented later.

## 4 RESULTS AND DISCUSSIONS

The Lyman- $\alpha$  absorption seen in the spectra of high- $z$  QSOs and the diminishing population of Lyman- $\alpha$  emitters suggest that the redshift  $z_{\text{re}} \sim 6$  is the most likely epoch where the process of H I reionization is completed. Therefore, we roughly assume that the post-reionization era to be  $z \leq 6$  and pre-reionization era to be  $z \geq 6$ . However, we consider the models of H I reionization where a very late reionization is allowed i.e.,  $z_{\text{re}} \geq 5.5$ . The results are discussed in the following sections.

### 4.1 Escape fraction in the post-reionization era

To constrain  $f_{\text{esc}}$  in the post-reionization era, we use  $\epsilon_{\nu}(z)$  as given in Eq. (13) which has contributions from both QSOs and galaxies. At any redshift  $z_0$ , the UVB depends on  $\epsilon_{\nu}$  at  $z \geq z_0$ . Therefore, we need  $f_{\text{esc}}$  at  $z > z_0$  to estimate the UVB at  $z_0$ . However, at  $z > 5.5$ , the mean free path of H I ionizing photons ( $\lambda_{\text{mfp}}$ ) is small enough ( $\lambda_{\text{mfp}} < 10$  pMpc; [Worseck et al. 2014b](#)) so that the UVB is essentially contributed by the local sources. Therefore, we start from redshift  $z_0 \sim 6$  and generate the UVB (and  $\Gamma_{\text{HI}}$ ) by taking  $f_{\text{esc}}(z > z_0)$  as a constant free parameter (by solving Eq. (3) with  $Q_{\text{HI}} = 1$ ). The  $f_{\text{esc}}(z_0)$  is then adjusted to generate the  $\Gamma_{\text{HI}}(z_0)$  that matches with the measurement at  $z_0$ . Once fixed at  $z_0 \sim 6$ , we use this  $f_{\text{esc}}(z \geq z_0)$  and calculate the UVB at a lower redshift  $z' < z_0$  by taking  $f_{\text{esc}}$  as a constant free parameter in a small redshift interval  $z' \leq z < z_0$  and fix its value to generate the  $\Gamma_{\text{HI}}(z')$  measurement. This gives the  $f_{\text{esc}}(z \geq z')$ . We repeat this procedure for lower  $z < z'$  down to  $z \sim 2$  and obtain the  $f_{\text{esc}}(z)$  over  $2 < z < 6$ . This method is identical to the progressive fitting method we used in [KS15b](#) to simultaneously obtain the  $A_{\text{FUV}}(z)$  and SFRD( $z$ ).

To obtain the  $f_{\text{esc}}(z)$ , we used following measurements of  $\Gamma_{\text{HI}}(z)$ . At  $2 < z < 5$ , we take the  $\Gamma_{\text{HI}}$  from [Becker & Bolton \(2013\)](#) along with the measurements by [Bolton & Haehnelt \(2007\)](#). These are obtained using the observed mean Lyman- $\alpha$  flux decrement, the opacity of H I ionizing photons and measurements of the IGM temperature by [Becker et al. \(2011\)](#). At  $z \sim 5$  and 6, we consider the  $\Gamma_{\text{HI}}$  obtained from the mean Lyman- $\alpha$  opacity by [Wytthe & Bolton \(2011\)](#) and from the QSO proximity effect by [Calverley et al. \(2011\)](#). These measurements are shown in the right panel of Fig. 3. We linearly interpolate these measurements over the redshift range  $5 < z < 6$ .

The resultant range in the required  $f_{\text{esc}}(z)$  and corresponding range in the  $\Gamma_{\text{HI}}(z)$  generated from it is shown in the Fig. 3. At lower redshifts  $z < 2$ , the  $f_{\text{esc}}$  can have values between 0 to 0.04 as demonstrated by us in [KS15a](#). For that, we have used the  $\Gamma_{\text{HI}}$  inferred by [Kollmeier et al. \(2014\)](#) and [Shull et al. \(2015\)](#) by calibrating their hydrodynamical simulations of the IGM to match the column density distribution of low- $z$  IGM reported by [Danforth et al. \(2016\)](#) (see also, [Wakker et al. 2015](#), for different method). Including this low- $z$   $f_{\text{esc}}$ , it is evident from Fig. 3 that for  $z < 3.5$ , the constant  $f_{\text{esc}}$  of 0 to 0.05 is sufficient to generate the measured  $\Gamma_{\text{HI}}(z)$ . This  $f_{\text{esc}}$  is consistent with the recent  $3 - \sigma$  upper limits on the average  $f_{\text{esc}}$  obtained by stacking the sample of galaxies used in respective studies at  $z < 0.9$  ([Grimes et al. 2009](#); [Bridge et al. 2010](#); [Leitet et al. 2013](#)) and at  $0.9 < z < 3.3$  ([Cowie et al. 2009](#); [Siana et al. 2010](#); [Vanzella et al. 2010](#); [Grazian et al. 2016](#)) as shown in the left panel of Fig. 3. These reported  $3 - \sigma$  upper limits are usually given in terms of relative escape fraction  $f_{\text{esc}}^{\text{rel}}$  that is related to the absolute escape fraction  $f_{\text{esc}}$  as following

$$f_{\text{esc}}^{\text{rel}} = \frac{(L_{\text{FUV}}/L_{\text{LyC}})_{\text{int}}}{(L_{\text{FUV}}/L_{\text{LyC}})_{\text{obs}}} \exp(\tau_{\text{IGM}}) = f_{\text{esc}} 10^{0.4A_{\text{FUV}}}, \quad (19)$$

where,  $\tau_{\text{IGM}}$  is the effective optical depth encountered by Lyman continuum photons (LyC,  $\lambda \leq 912 \text{ \AA}$ ) while travelling from the source to the earth due to the IGM. We convert these  $f_{\text{esc}}^{\text{rel}}$  into absolute escape fraction  $f_{\text{esc}}$  by taking into account the  $A_{\text{FUV}}$  used in our galaxy model (see Eq. 15) and

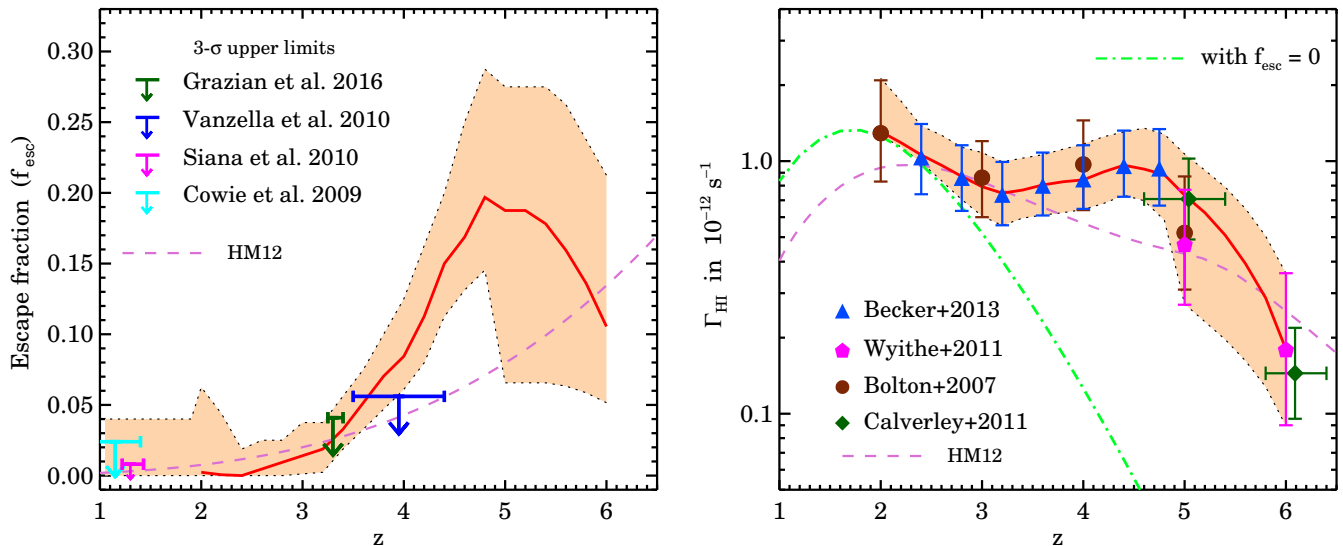


**Figure 3.** The derived constraints on the  $f_{\text{esc}}(z)$  (left-hand panel) from the measurements of  $\Gamma_{\text{HI}}(z)$  (right-hand panel). The  $\Gamma_{\text{HI}}(z)$  measurements are taken from Becker & Bolton (2013); Bolton & Haehnelt (2007); Calverley et al. (2011); Wyithe & Bolton (2011). Green dot-dash curve in right panel shows  $\Gamma_{\text{HI}}(z)$  obtained using only  $\epsilon_{912}^Q(z)$  given in Eq. (14) i.e with  $f_{\text{esc}} = 0$ . Shaded region in both panels show the range in the  $f_{\text{esc}}(z)$  (on left) and corresponding  $\Gamma_{\text{HI}}(z)$  (on right). Solid red line shows mean  $f_{\text{esc}}(z)$  that reproduces the mean  $\Gamma_{\text{HI}}(z)$  measurements. We also show  $3\text{-}\sigma$  upper limits on mean  $f_{\text{esc}}(z)$  from various observations (Cowie et al. 2009; Siana et al. 2010; Vanzella et al. 2010; Grazian et al. 2016). The range of  $f_{\text{esc}}(z)$  obtained here is consistent with these upper limits at  $z < 3.5$ . However  $f_{\text{esc}}(z)$  needs a steep rise from  $z \sim 3$  to  $z \sim 5$  from  $\sim 0.05$  to  $\sim 0.2$  to match a nearly constant  $\Gamma_{\text{HI}}(z)$  over this  $z$ -range. We also show the  $f_{\text{esc}}(z)$  used by HM12 and corresponding  $\Gamma_{\text{HI}}(z)$ . See the text for more details.

the difference between the ratio of the intrinsic luminosities  $(L_{\text{FUV}}/L_{\text{LyC}})_{\text{int}}$  assumed in these references and the one we get from our model.

On the contrary to  $z < 3.5$ , at  $3.5 < z < 4.8$ , the required  $f_{\text{esc}}(z)$  needs a steep rise up to  $\sim 0.15$  to  $0.25$  for maintaining the observed trend of a nearly constant  $\Gamma_{\text{HI}}(z)$ . The main reason behind this required rapid increase in  $f_{\text{esc}}$  from  $z \sim 3.5$  to  $z \sim 5$  is that the galaxies need to produce large number of H I ionizing photons to compensate for the rapid decline in the fiducial QSO emissivity by a factor  $\sim 10$ , and to maintain the nearly constant  $\Gamma_{\text{HI}}(z)$  measured in this  $z$  range. A similar but less rapid increase in  $f_{\text{esc}} \propto (1+z)^{3.4}$  was also required by HM12 as shown in Fig. 3. However, note that the  $\Gamma_{\text{HI}}(z)$  used by HM12 was from the previous measurements of Becker et al. (2007) that decreased by a factor of  $\sim 2$  from  $z = 3$  to  $5$  (see, Fig. 3).

The measured  $\Gamma_{\text{HI}}$  at  $z \sim 6$  is a factor of 4 to 10 times smaller than the  $\Gamma_{\text{HI}}$  at  $z \sim 5$ . This decrease in  $\Gamma_{\text{HI}}$  from  $z \sim 5$  to  $z \sim 6$  is mainly because of the increasing opacity of the IGM (Inoue et al. 2014). We find that the  $f_{\text{esc}}$  of 0.05 to 0.2 is required at  $z = 6$ . It will be interesting to see what values of  $f_{\text{esc}}$  at  $z \geq 6$  are allowed by the H I reionization process. We explore this in the following section.

#### 4.2 Escape fraction in the pre-reionization era

In the pre-reionization era, in absence of any observational constraints or theoretical inputs, we consider models of H I reionization with a constant  $f_{\text{esc}}$  at  $z \geq z_{\text{re}}$ . We extrapolate our fiducial SFRD( $z$ ) up to  $z \sim 13$  and start the pro-

cess of reionization from there.<sup>4</sup> We find that  $\tau_{\text{el}}$  measurements of Planck Collaboration et al. (2015) allow the minimum constant  $f_{\text{esc}}$  of 0.14 where the reionization completes at  $z_{\text{re}} = 5.5$  and a maximum constant  $f_{\text{esc}}$  as high as 0.8 where the reionization completes at  $z_{\text{re}} = 8.8$ . For different  $f_{\text{esc}}$ , we obtain  $Q_{\text{HII}}(z)$  and evaluate  $\tau_{\text{el}}$ . Results for some of these models are shown in Fig. 4. We find that the  $Q_{\text{HII}}(z)$  obtained for the constant  $f_{\text{esc}}$  range from 0.14 to 0.22 satisfies the recently inferred mean H I fraction in the IGM at  $z = 5.9$  by McGreer et al. (2015) using the dark pixel statistic in high- $z$  QSO spectra and at  $z \sim 7$  and  $z \sim 8$  by Schenker et al. (2014) using the observations of the diminishing fraction of high- $z$  Lyman- $\alpha$  emitters (see Fig. 4 left panel). As explained earlier, this range of  $f_{\text{esc}}$  is also consistent with the  $f_{\text{esc}}$  required to generate  $\Gamma_{\text{HI}}$  measurements at  $z \sim 6$ . (See appendix A for the discussion on the  $\Gamma_{\text{HI}}(z)$  and  $C(z)$  at  $z \geq z_{\text{re}}$ .) The recent measurements of  $\tau_{\text{el}}$  from Planck satellite along with the updated SFRD( $z$ ) has helped us to reduce the  $f_{\text{esc}}$  as small as 0.14 (see also Mashian et al. 2016; Mitra et al. 2015; Robertson et al. 2015; Bouwens et al. 2015a; Vangioni et al. 2015) from very high values of  $f_{\text{esc}}$  inferred previously from  $\tau_{\text{el}}$  reported by WMAP (such as, HM12, Choudhury & Ferrara 2005; Kuhlen & Faucher-Giguère 2012; Fontanot et al. 2014). We consider a model with a constant  $f_{\text{esc}} = 0.18$  as our fiducial model where the reionization completes at  $z_{\text{re}} = 5.9$  and  $\tau_{\text{el}} = 0.055$ .

Combining the  $f_{\text{esc}}$  constraints from  $z \leq 6$  (as shown

<sup>4</sup> We note that, any starting redshift  $z \geq 13$  has negligible effect on the  $z_{\text{re}}$  for the models with constant  $f_{\text{esc}} < 0.4$ .

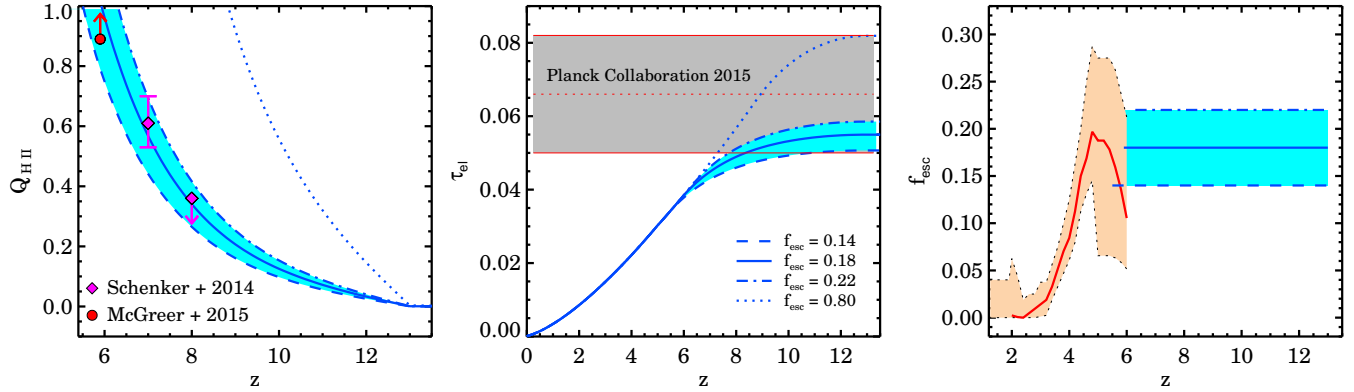


**Figure 4.** The range in  $Q_{\text{HII}}(z)$  (left-hand panel) and the range in corresponding  $\tau_{\text{el}}(z)$  (central panel) obtained by using the constant  $f_{\text{esc}}(z)$  at  $z \geq z_{\text{re}}$  (right-hand panel; shaded region in cyan) are shown. We find that the  $f_{\text{esc}} = 0.14$  ( $z_{\text{re}} = 5.5$  and  $\tau_{\text{el}} = 0.05$ ) to  $f_{\text{esc}} = 0.22$  ( $z_{\text{re}} = 6.3$  and  $\tau_{\text{el}} = 0.059$ ) are consistent with the recent  $\tau_{\text{el}}$  constraints from Planck (gray shaded region in central panel) and measurements of mean H I fraction (points in the left-hand panel) by Schenker et al. (2014) and McGreer et al. (2015). Maximum allowed  $f_{\text{esc}}$  only from  $\tau_{\text{el}}$  is 0.8 (with  $z_{\text{re}} = 8.8$  and  $\tau_{\text{el}} = 0.082$ ). In the right-hand panel we also show the constraints on  $f_{\text{esc}}(z)$  at  $z < 6$  obtained in Section 4 (see Fig. 3). Note that, to simultaneously reionize the Universe and obtain the  $\Gamma_{\text{HI}}(z)$  measurements, the  $f_{\text{esc}}(z)$  needs a rapid increase from  $\sim 0.05$  at  $z < 3.5$  to at least  $\sim 0.15$  at  $z \sim 5.5$ .

in the right panel of Fig. 4), an evolution in  $f_{\text{esc}}(z)$  of at least a factor 3 from 0.05 to 0.15 is required from  $z \sim 3.5$  to  $z \sim 5.5$  to simultaneously satisfy recent observational constraints on H I reionization and  $\Gamma_{\text{HI}}$  measurements at all  $z$ . This redshift range ( $3.5 < z < 5.5$ ) corresponds to an elapsed time of  $7.5 \times 10^8$  yr, only 4 times the dynamical time scale at  $z = 4.5$  (Samui et al. 2007). This trend in  $f_{\text{esc}}$  implies that the population of galaxies at  $z > 3.5$  are different from their local counterparts. It may either mean that the high- $z$  galaxies are more porous than the low- $z$  ones or the stellar efficiency to generate large amount of H I ionizing photons has increased via rapid evolution in IMF, metallicity or the rotations in stars (Topping & Shull 2015). However, in the latter case, these parameters should evolve rapidly to provide a higher ratio of  $L_{\text{LyC}}$  to  $L_{\text{FUV}}$  (see Eq. 19). For example, changing metallicity from  $0.4Z_{\odot}$  to  $0.005Z_{\odot}$  increases the above ratio only by  $< 10\%$ . Therefore, a rapid evolution in metallicity alone will not provide rapid increase in  $f_{\text{esc}}$ . Many theoretical studies predict increasing  $f_{\text{esc}}$  with  $z$  via various mechanisms such as the luminosity dependent  $f_{\text{esc}}$  (Ferrara & Loeb 2013), a large  $f_{\text{esc}}$  from faint low mass galaxies whose number density increases with  $z$  (Alvarez et al. 2012; Cai et al. 2014; Fontanot et al. 2014), the supernovae dominated primordial galaxies (Yajima et al. 2009) and evolution in the covering factors of clumps in the interstellar medium (Fernandez & Shull 2011; Roy et al. 2015). However, the main difficulty of using these mechanisms to explain our results is that the corresponding physical changes in the properties of galaxies have to occur over a very short period of time.

There is a growing evidence of  $f_{\text{esc}}$  being low even at high  $z$ . The earlier reported measurements of high  $f_{\text{esc}}$  values (such as, Steidel et al. 2001; Shapley et al. 2006) are found to be dominated by the contamination from low- $z$  interlopers (Siana et al. 2015; Mostardi et al. 2015; Grazian et al. 2016). In addition, simulations of Ma et al. (2015) show that the time average value of  $f_{\text{esc}}$  is  $\leq 0.05$  without any strong dependence on the properties of galaxies and redshift. In

light of these, we now explore the models with low  $f_{\text{esc}}$  of H I ionizing photons from galaxies. This will require an enhanced contribution from QSOs to H I ionizing photons at  $z > 3.5$ . The QSO emissivity at  $z > 3.5$  is fairly uncertain because of the ill-constrained faint end slope and the characteristic turnover luminosity  $L^*$  of the QLFs. This allows us some room for the exploration.

### 4.3 Prediction for optimal QSO model: $\epsilon_{912}^Q(z)$

Giallongo et al. (2015) discovered 22 faint active galactic nuclei (AGN) candidates at  $4 < z < 6$  through multi-wavelength observations of high- $z$  galaxies. The QLFs derived using these AGN have  $L^*$  an order of magnitude smaller and number density  $\phi^*$  at least two orders of magnitude higher as compared to other QLFs (such as, Masters et al. 2012; McGreer et al. 2015; Kashikawa et al. 2015). This eventually provides an emissivity of the H I ionizing photons that is  $\sim 10$  to  $\sim 50$  times higher than the other QLFs, assuming the usual escape fraction of unity and the same SEDs that one takes for the bright QSOs. Interestingly, as shown by Giallongo et al. (2015) the emissivity obtained in this way can generate the  $\Gamma_{\text{HI}}(z)$  measurements without requiring any galaxy contribution at  $4 < z < 6$ . Motivated by these QLF measurements, we take the H I ionizing QSO emissivity,  $\epsilon_{912}^Q(z)$ , as a free parameter at  $2 < z < 6$  and constrain its values using  $\Gamma_{\text{HI}}(z)$  measurements by fixing the  $f_{\text{esc}}$  from galaxies to be in the range of 0.02 to 0.05.

We follow the same method described in Section 4.1, where instead of  $f_{\text{esc}}$  now we find  $\epsilon_{912}^Q(z)$  consistent with the  $\Gamma_{\text{HI}}$  measurements by assuming a constant  $f_{\text{esc}}$  of 0.02 and 0.05. The results of this exercise are shown in Fig. 5 along with the  $\epsilon_{912}^Q(z)$  used here (Eq. 14) from compilation of KS15a and from the QLF of Giallongo et al. (2015). For a constant  $f_{\text{esc}} = 0.05$ , at  $z < 3.5$  the minimum required  $\epsilon_{912}^Q(z)$  goes to zero since galaxies are sufficient to generate the measured  $\Gamma_{\text{HI}}$  down to its  $1-\sigma$  value (see the horizontal striped region in Fig. 5). However, at  $z > 3.5$  the required  $\epsilon_{912}^Q(z)$  is higher suggesting a need for an increase in the

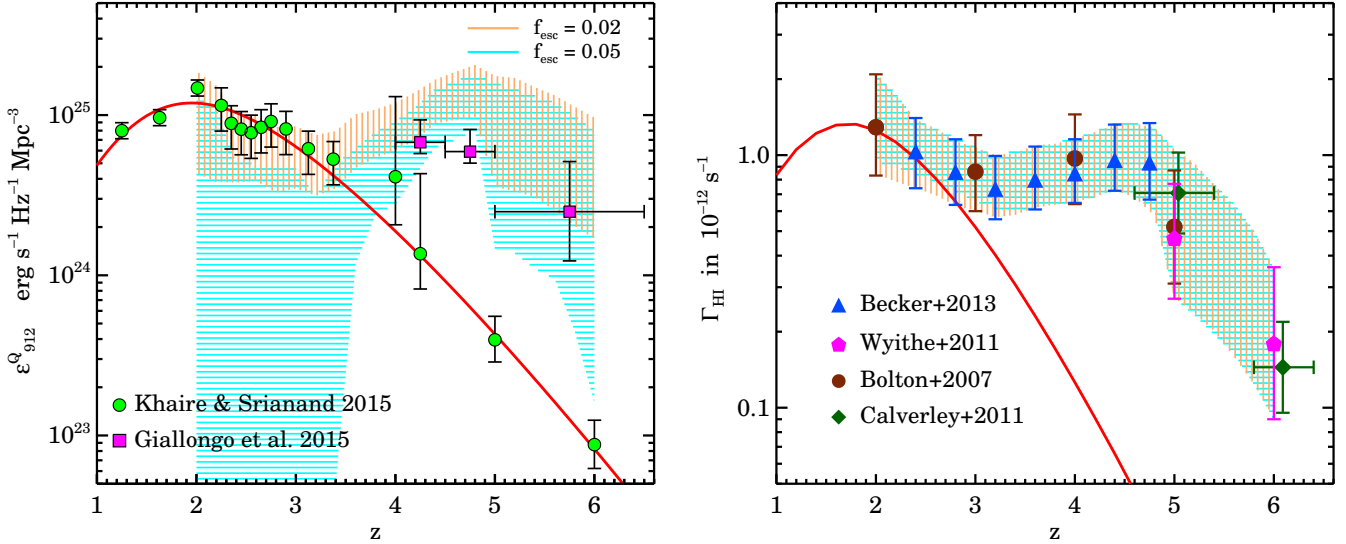


**Figure 5.** Left-hand panel: Constraints on the  $\epsilon_{912}^Q(z)$  at  $z > 2$  obtained assuming a constant  $f_{\text{esc}} = 0.02$  and  $0.05$  of H I ionizing photons from galaxies. The required range of  $\epsilon_{912}^Q(z)$  when  $f_{\text{esc}} = 0.05$  is shown by horizontal stripes. Notice at  $2 < z < 3.5$  the  $f_{\text{esc}} = 0.05$  is sufficient to generate  $\Gamma_{\text{HI}}$  measurements down to its  $1-\sigma$  low value purely from galaxies and no additional contribution is needed from QSOs. Allowed range of  $\epsilon_{912}^Q(z)$  when  $f_{\text{esc}} = 0.02$  is shown by vertical stripes. The *green circles* are from compilation by *KS15a* and *red curve* is a fit through them as given in Eq. (14). *Magenta squares* are from QLFs of *Giallongo et al. (2015)*. Right-hand Panel: The corresponding  $\Gamma_{\text{HI}}(z)$  measurements are shown (see Fig. 3). The description of horizontal and vertical stripes is same as given for the left panel. *Red curve* shows  $\Gamma_{\text{HI}}$  computed using  $\epsilon_{912}^Q(z)$  fit shown in the left panel with  $f_{\text{esc}} = 0$ .

fiducial  $\epsilon_{912}^Q(z)$  by at least a factor of  $\sim 2$  to  $\sim 8$ . For  $f_{\text{esc}} = 0.02$ , there are more stringent constraints on the  $\epsilon_{912}^Q(z)$ . At  $z < 3.5$  our fiducial  $\epsilon_{912}^Q(z)$  is consistent with the allowed range (see the vertical striped region in Fig. 5). However, at  $z > 3.5$ , there is a need of at least a factor of  $\sim 4$  to  $\sim 20$  rise in our fiducial  $\epsilon_{912}^Q(z)$ . Note that, At  $z > 4$ , the QLFs used to obtain the  $\epsilon_{912}^Q(z)$  in *KS15a* are taken from *Glikman et al. (2011)*; *Masters et al. (2012)*; *McGreer et al. (2013)*; *Kashikawa et al. (2015)*, where the faint end slopes have large uncertainties. The  $\epsilon_{912}^Q(z)$  from *Glikman et al. (2011)* at  $z \sim 4$  and *Giallongo et al. (2015)* at  $z \geq 4$  satisfy the allowed range when we assume  $f_{\text{esc}}$  from 0.02 to 0.05.

#### 4.4 H I reionization with only QSOs

The population of faint AGN detected in the recent multi-wavelength surveys (*Glikman et al. 2011*; *Fiore et al. 2012*; *Civano et al. 2011*) hints towards the possibility that the QSOs may be dominant sources of reionization (*Giallongo et al. 2012*). In light of these, we explore a possibility where only QSOs reionize the Universe. We consider a range of QSO emissivities at  $z > z_{\text{re}}$  which can reionize the Universe and at the same time remaining consistent with the emissivity of *Giallongo et al. (2015)* and  $\tau_{\text{el}}$  measurements from *Planck Collaboration et al. (2015)*. We parametrize the range in QSO emissivity at  $z > 4$  as a power law  $\epsilon_{912}^Q(z) = 9.55 \times 10^{24} [(1+z)/5]^\gamma \text{ erg s}^{-1} \text{ Hz}^{-1} \text{ Mpc}^{-3}$  and find that the  $\gamma$  can have values  $-2$  to  $-2.6$ . For this range in  $\epsilon_{912}^Q$ , the obtained  $Q_{\text{HI}}(z)$  evolution and the  $\tau_{\text{el}}(z)$  are shown in the Fig. 6. Similar to the previous model, the resultant  $Q_{\text{HI}}(z)$  is also consistent with the mean H I fraction measurements of *Schenker et al. (2014)* and *McGreer et al.*

(2015). For  $\gamma = -2.0$  (respectively  $-2.6$ ), the H I reionization completes at  $z_{\text{re}} = 5.8$  (respectively 5.5) and it provides  $\tau_{\text{el}} = 0.055$  (respectively 0.05).

Similar calculations were recently presented by *Madau & Haardt (2015)* (hereafter *MH15*), where they obtain the  $z_{\text{re}} \sim 5.7$  with  $\tau_{\text{el}} = 0.056$ . A small difference between our and their models arises from the differences in the SEDs ( $\alpha$ , See Eq. 13) of QSOs and the clumping factor used. We take  $\alpha = -1.4$  following *Stevens et al. (2014)* which gives 20% higher  $\dot{n}$  as compared to the one obtained by *MH15* with  $\alpha = -1.7$  following *Lusso et al. (2015)*. The differences in clumping factors are shown in appendix A. Following the exact prescription given by *MH15* to calculate the contribution of QSOs at  $z > 5$  to the unresolved X-ray background, we find that the  $J_\nu$  at 2 keV is  $1.32 \times 10^{-27}$  (respectively  $1.04 \times 10^{-27}$ )  $\text{erg cm}^{-2} \text{ s}^{-1} \text{ Hz}^{-1} \text{ Sr}^{-1}$  for our emissivity models with  $\gamma = -2.0$  (respectively  $-2.6$ ) that is nearly 45% (respectively 35%) of the total X-ray background derived by *Moretti et al. (2012)*. Therefore, the emissivity of QSOs taken by us does not overproduce the unresolved X-ray background. It is still valid, even if we take the factor  $R_{\text{HI}}$ , the correction factor to estimate the obscured fraction of AGN, equal to 4 (see for e.g. *Haardt & Salvaterra 2015*; *Merloni et al. 2014*) instead of 2 as taken by *MH15*.

Till now, following *Giallongo et al. (2015)* and *MH15*, we have used a luminosity independent SED ( $\alpha = -1.4$ ) to estimate the emissivities from QLF. However, when faint AGN are included, the QSO luminosity extends over a wide range and therefore any correlation between the QSO luminosity and SED may become important. We provide a simple way to estimate the luminosity-dependent  $\alpha$  via a tight correlation found between the optical luminosity at 2500 Å (i.e.  $L_{\nu 2500}$ ) and the optical to X-ray (2 keV) spectral index,  $\alpha_{\text{ox}}$ .

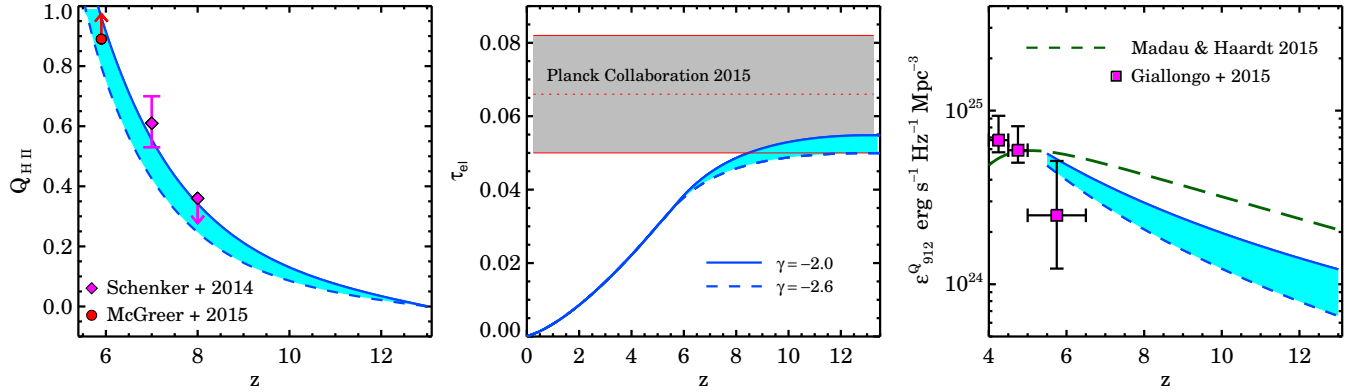


**Figure 6.** The range in  $Q_{\text{HII}}(z)$  (left-hand panel) and the range in corresponding  $\tau_{\text{el}}(z)$  (central panel) obtained by using emissivity of QSOs (right-hand panel; shaded region in cyan) with no contribution from galaxies (i.e.  $f_{\text{esc}} = 0$ ). We parametrize the QSO emissivity at 912 Å with a power-law as  $\epsilon_{912}^Q(z) = 9.55 \times 10^{24} [(1+z)/5]^\gamma \text{ erg s}^{-1} \text{ Hz}^{-1} \text{ Mpc}^{-3}$  and find that the  $\gamma$  can have values  $-2$  (solid line, right-hand panel) to  $-2.6$  (dash line, right-hand panel) that is consistent with the QLFs by Giallongo et al. (2015) (magenta squares; right-hand panel),  $\tau_{\text{el}}$  constraints from Planck (gray shade; central panel) and the mean H I fraction by Schenker et al. (2014) and McGreer et al. (2015) (points in left-hand panel). For comparison, we also show the  $\epsilon_{912}^Q$  emissivity used by MH15 (green long dash; right-hand panel).  $\epsilon_{912}^Q(z)$  used by us is lower than them. See the text for more details.

This is usually written as  $\alpha_{\text{ox}} = AL_{\nu 2500} - B$ , where  $A = 0.154$  and  $B = -3.176$  as reported by Lusso et al. (2010), and  $A = 0.065$  and  $B = -0.509$  as reported by Stalin et al. (2010). We have used a piece-wise SED to obtain the ionizing emissivity from QLFs (in KS15a) by taking  $L_\nu \propto \nu^{\alpha_0}$  with  $\alpha_0 = -0.5$  at  $\lambda > 2000$  Å,  $\alpha_0 = -0.8$  at  $2000 > \lambda > 1000$  Å and  $\alpha_0 = \alpha$  at  $1000 > \lambda > 24.8$  Å (Stevens et al. 2014), and  $\alpha_0 = -0.9$  at  $\lambda < 24.8$  Å (Nandra & Pounds 1994). This coupled with  $\alpha_{\text{ox}}$  to give a consistent ratio of luminosities at 2500 Å and 2 keV results into  $\alpha = 1.1\alpha_{\text{ox}}$ . This relation along with the correlation between  $\alpha_{\text{ox}}$  and  $L_{\nu 2500}$  provides a luminosity dependent  $\alpha$ . We use this and estimate the  $\epsilon_{\nu 912}^Q$  from the QLF of Giallongo et al. (2015). This gives a maximum of 30 (respectively 20)% lower  $\dot{n}$  and 16 (respectively 13)% lower  $\Gamma_{\text{HI}}$  when we use  $\alpha_{\text{ox}}$  and  $L_{\nu 2500}$  correlation from Stalin et al. (2010) (respectively Lusso et al. 2010). This change in  $\dot{n}$  and  $\Gamma_{\text{HI}}$  allows  $\gamma$  to have minimum value of  $-2.5$  instead of  $-2.6$ .

The model presented here relies on the QLFs reported by Giallongo et al. (2015). However, a similar study performed by Weigel et al. (2015) and Georgakakis et al. (2015) could not confirm the detection of large number of faint AGN. Georgakakis et al. (2015) estimated X-ray QLFs at  $3 < z < 5$  and show that the upper limits on the H I ionizing emissivity from their QLFs can not generate the measured  $\Gamma_{\text{HI}}$  at  $z > 4$ . More observations of similar nature and tight constraints on the SEDs of the faint AGN along with their escape fraction of UV photons are required to confirm the results of Giallongo et al. (2015).

## 5 SUMMARY

We study the contribution of QSOs and galaxies to the H I ionizing emissivity as a function of  $z$  that can reionize the Universe satisfying the  $\tau_{\text{el}}$  constraints from the recent CMB measurements and consistently reproduce the  $\Gamma_{\text{HI}}$  measurements at  $z \leq 6$ . For this, we use a radiative transfer code developed by us to estimate the UV background

with the updated QSO emissivity (KS15a) and star formation rate density (KS15b). We use updated H I column density distribution from Inoue et al. (2014) at  $z < 6$  and the one computed using hydrodynamical simulations in the preionization era.

We constrain the escape fraction ( $f_{\text{esc}}$ ) of H I ionizing photons from galaxies as a function of  $z$ . We find a constant  $f_{\text{esc}} = 0.14 - 0.22$  is sufficient to reionize the Universe satisfying the recent observational constraints (Planck Collaboration et al. 2015; McGreer et al. 2015; Schenker et al. 2014). We show that, a constant  $f_{\text{esc}} \sim 0 - 0.05$  is sufficient to obtain the measured  $\Gamma_{\text{HI}}$  at  $z \leq 3.5$ . However, between  $z \sim 3.5$  and  $5.5$  (i.e over an elapsed time of  $\sim 7.5 \times 10^8$  yr) a sharp increase in  $f_{\text{esc}}$  of at least a factor  $\sim 3$  is required. This is mainly because of the rapid decline in the QSO emissivity at  $z \geq 3$  and the requirement to obtain a nearly constant  $\Gamma_{\text{HI}}(z)$ .

The required rapid increase in  $f_{\text{esc}}$  may imply either the high- $z$  galaxies are more porous than the low- $z$  ones or the stellar efficiency to generate large amount of H I ionizing photons has increased with a rapid evolution in the properties of galaxies. Confirming this by direct measurements of increasing  $f_{\text{esc}}$  or rapidly evolving nebular emission line ratios over  $3.5 < z < 5.5$  will favor the galaxy dominated UV background at high- $z$ . However, the main problem with this scenario is that all the physical changes have to occur over a very short time-scale ( $\sim 4$  times the dynamical time scale at  $z = 4.5$ ). This may not be naturally obtained in the structure formation models (see for e.g. Ma et al. 2015). In addition, there is a growing evidence of  $f_{\text{esc}}$  being low even at high  $z$ . The earlier reported measurements of high  $f_{\text{esc}}$  values are found to be dominated by the contamination from low- $z$  interlopers (Siana et al. 2015; Mostardi et al. 2015; Grazian et al. 2016).

We further explore the possibility of QSOs dominating the H I ionization throughout the history of the Universe. We estimate the required QSO emissivities assuming a constant  $f_{\text{esc}} = 0.02 - 0.05$ . Under this scenario, at  $z > 3.5$  our

fiducial QSO emissivity needs to be enhanced by at least a factor of  $\sim 4$  to  $\sim 20$  to obtain the measured  $\Gamma_{\text{HI}}$ . However, this enhanced emissivity is consistent with the QLF obtained by [Giallongo et al. \(2015\)](#). With a simple extrapolation of this emissivity to higher redshifts, we show that QSOs alone can reionize the Universe satisfying the observational constraints (as also shown by [MH15](#)). Note that in this case, the QSO emissivity is dominated by the low luminosity AGN with black hole masses in the range  $10^6$ – $10^8 M_{\odot}$  probably hosted by low mass (i.e.  $10^9 M_{\odot}$ ) galaxies. However, models of black hole formation at high- $z$  show that the strong stellar feedback may hinder black hole formation in low mass galaxies (see for e.g. [Dubois et al. 2015](#)). Therefore, independent observational confirmations of the findings of [Giallongo et al. \(2015\)](#) are important (see [Weigel et al. 2015](#); [Georgakakis et al. 2015](#), for non-confirmation) to further investigate the QSO dominated UV background scenarios at  $z > 3.5$ .

The QSO-dominated H I reionization can also lead to a range of observable signatures. The topology of the ionized bubbles will be distinctly different as compared to galaxy-dominated models. This will change the predictions of 21 cm signals that can be searched with future experiments. This will also affect the constraints on reionization obtained from the observed decrease in the density of Lyman- $\alpha$  emitters at  $z > 6$  (such as [Mesinger & Furlanetto 2008](#); [Choudhury et al. 2015](#)). The AGN contamination in high- $z$  Lyman- $\alpha$  emitter samples should also show an increasing trend with  $z$ . In principle, the highly ionized regions around these numerous faint AGN can be studied using the presence of the He II  $\lambda 1640 \text{ \AA}$  emission line. The thermal history of the IGM will be affected because of the hard SEDs of QSOs, the additional heating from the He II ionization in the near zones of QSOs ([Bolton et al. 2012](#); [Padmanabhan et al. 2014](#)) and the X-ray heating ([Venkatesan et al. 2001](#)). The inferred redshift of He II reionization and the interpretation of observed He II Lyman- $\alpha$  effective optical depths ([Worseck et al. 2014a](#)) will be significantly different ([Furlanetto & Dixon 2010](#); [Compostella et al. 2014](#), [MH15](#)).

All these emphasize a need for improved observational constraints and a careful modelling of the above-mentioned observables under both galaxy- and QSO-dominated UV background scenarios. The improved  $\Gamma_{\text{HI}}$  measurements with tight constraints on IGM temperature and density are also needed to further study the relative contribution of QSOs and galaxies to UV background.

## ACKNOWLEDGEMENT

We thank anonymous referee for the useful comments on the manuscript. We thank V. Springel for providing P-GADGET3 code. The simulations were performed using the Perseus cluster of the IUCAA High Performance Computing Centre. We thank A. Paranjape for the useful comments on the manuscript. V. Khaire acknowledges support from the CSIR.

## REFERENCES

Alvarez M. A., Finlator K., Trenti M., 2012, *ApJ*, 759, L38

- Barger K. A., Haffner L. M., Bland-Hawthorn J., 2013, *ApJ*, 771, 132
- Barkana R., Loeb A., 2001, *PhR*, 349, 125
- Becker G. D., Bolton J. S., 2013, *MNRAS*, 436, 1023
- Becker G. D., Rauch M., Sargent W. L. W., 2007, *ApJ*, 662, 72
- Becker G. D., Bolton J. S., Haehnelt M. G., Sargent W. L. W., 2011, *MNRAS*, 410, 1096
- Becker G. D., Hewett P. C., Worseck G., Prochaska J. X., 2013, *MNRAS*, 430, 2067
- Behroozi P. S., Wechsler R. H., Conroy C., 2013, *ApJ*, 770, 57
- Benson A., Venkatesan A., Shull J. M., 2013, *ApJ*, 770, 76
- Bolton J. S., Haehnelt M. G., 2007, *MNRAS*, 382, 325
- Bolton J. S., Haehnelt M. G., 2013, *MNRAS*, 429, 1695
- Bolton J. S., Becker G. D., Raskutti S., Wyithe J. S. B., Haehnelt M. G., Sargent W. L. W., 2012, *MNRAS*, 419, 2880
- Bolton J. S., Haehnelt M. G., Warren S. J., Hewett P. C., Mortlock D. J., Venemans B. P., McMahon R. G., Simpson C., 2011, *MNRAS*, 416, L70
- Borthakur S., Heckman T. M., Leitherer C., Overzier R. A., 2014, *Science*, 346, 216
- Boutsia K. et al., 2011, *ApJ*, 736, 41
- Bouwens R. J., Illingworth G. D., Oesch P. A., Caruana J., Holwerda B., Smit R., Wilkins S., 2015a, *ApJ*, 811, 140
- Bouwens R. J. et al., 2012, *ApJ*, 754, 83
- Bouwens R. J. et al., 2015b, *ApJ*, 803, 34
- Bridge C. R. et al., 2010, *ApJ*, 720, 465
- Cai Z. Y., Lapi A., Bressan A., De Zotti G., Negrello M., Danese L., 2014, *ApJ*, 785, 65
- Calverley A. P., Becker G. D., Haehnelt M. G., Bolton J. S., 2011, *MNRAS*, 412, 2543
- Cen R., Kimm T., 2015, *ApJ*, 801, L25
- Choudhury T. R., 2009, *Current Science*, 97, 841
- Choudhury T. R., Ferrara A., 2005, *MNRAS*, 361, 577
- Choudhury T. R., Puchwein E., Haehnelt M. G., Bolton J. S., 2015, *MNRAS*, 452, 261
- Civano F. et al., 2011, *ApJ*, 741, 91
- Compostella M., Cantalupo S., Porciani C., 2014, *MNRAS*, 445, 4186
- Conroy C., Kratter K. M., 2012, *ApJ*, 755, 123
- Cowie L. L., Barger A. J., Trouille L., 2009, *ApJ*, 692, 1476
- Croom S. M. et al., 2009, *MNRAS*, 399, 1755
- Danforth C. W. et al., 2016, *ApJ*, 817, 111
- Dove J. B., Shull J. M., 1994, *ApJ*, 423, 196
- Dubois Y., Volonteri M., Silk J., Devriendt J., Slyz A., Teyssier R., 2015, *MNRAS*, 452, 1502
- Fan X. et al., 2006, *aj*, 132, 117
- Fardal M. A., Giroux M. L., Shull J. M., 1998, *aj*, 115, 2206
- Faucher-Giguère C. A., Lidz A., Zaldarriaga M., Hernquist L., 2009, *ApJ*, 703, 1416
- Fernandez E. R., Shull J. M., 2011, *ApJ*, 731, 20
- Ferrara A., Loeb A., 2013, *MNRAS*, 431, 2826
- Finkelstein S. L. et al., 2015, *ApJ*, 810, 71
- Fiore F. et al., 2012, *A&A*, 537, A16
- Fontanot F., Cristiani S., Pfrommer C., Cupani G., Vanzella E., 2014, *MNRAS*, 438, 2097
- Fujita A., Martin C. L., Mac Low M. M., Abel T., 2003, *ApJ*, 599, 50
- Furlanetto S. R., Dixon K. L., 2010, *ApJ*, 714, 355
- Georgakakis A. et al., 2015, *MNRAS*, 453, 1946
- Giallongo E., Menci N., Fiore F., Castellano M., Fontana A., Grazian A., Pentericci L., 2012, *ApJ*, 755, 124
- Giallongo E. et al., 2015, *A&A*, 578, A83
- Glikman E., Djorgovski S. G., Stern D., Dey A., Jannuzi B. T., Lee K. S., 2011, *ApJ*, 728, L26
- Gnedin N. Y., Kravtsov A. V., Chen H. W., 2008, *ApJ*, 672, 765
- Gordon K. D., Clayton G. C., Misselt K. A., Landolt A. U., Wolff M. J., 2003, *ApJ*, 594, 279

- Goto T., Utsumi Y., Hattori T., Miyazaki S., Yamauchi C., 2011, MNRAS, 415, L1
- Grazian A. et al., 2016, A&A, 585, A48
- Grimes J. P. et al., 2009, ApJS, 181, 272
- Haardt F., Madau P., 1996, ApJ, 461, 20
- Haardt F., Madau P., 2012, ApJ, 746, 125
- Haardt F., Salvaterra R., 2015, A&A, 575, L16
- Hinshaw G. et al., 2013, ApJS, 208, 19
- Inoue A. K., Iwata I., Deharveng J. M., 2006, MNRAS, 371, L1
- Inoue A. K., Shimizu I., Iwata I., Tanaka M., 2014, MNRAS, 442, 1805
- Iwata I. et al., 2009, ApJ, 692, 1287
- Kashikawa N. et al., 2015, ApJ, 798, 28
- Khairé V., Srianand R., 2013, MNRAS, 431, L53
- Khairé V., Srianand R., 2015a, MNRAS, 451, L30
- Khairé V., Srianand R., 2015b, ApJ, 805, 33
- Kim T. S., Partl A. M., Carswell R. F., Müller V., 2013, A&A, 552, A77
- Kimm T., Cen R., 2014, ApJ, 788, 121
- Kollmeier J. A. et al., 2014, ApJ, 789, L32
- Kroupa P., 2001, MNRAS, 322, 231
- Kuhlen M., Faucher-Giguère C. A., 2012, MNRAS, 423, 862
- Larson D. et al., 2011, ApJS, 192, 16
- Leitet E., Bergvall N., Hayes M., Linné S., Zackrisson E., 2013, A&A, 553, A106
- Leitherer C. et al., 1999, ApJS, 123, 3
- Lusso E., Worseck G., Hennawi J. F., Prochaska J. X., Vignali C., Stern J., O’Meara J. M., 2015, MNRAS, 449, 4204
- Lusso E. et al., 2010, A&A, 512, A34
- Ma X., Kasen D., Hopkins P. F., Faucher-Giguère C. A., Quataert E., Kereš D., Murray N., 2015, MNRAS, 453, 960
- Madau P., Dickinson M., 2014, ARAA, 52, 415
- Madau P., Haardt F., 2015, ApJ, 813, L8
- Madau P., Haardt F., Rees M. J., 1999, ApJ, 514, 648
- Mashian N., Oesch P. A., Loeb A., 2016, MNRAS, 455, 2101
- Masters D. et al., 2012, ApJ, 755, 169
- McGreer I. D., Mesinger A., D’Odorico V., 2015, MNRAS, 447, 499
- McGreer I. D. et al., 2013, ApJ, 768, 105
- McLeod D. J., McLure R. J., Dunlop J. S., Robertson B. E., Ellis R. S., Targett T. A., 2015, MNRAS, 450, 3032
- Meiksin A., White M., 2003, MNRAS, 342, 1205
- Merloni A. et al., 2014, MNRAS, 437, 3550
- Mesinger A., Furlanetto S. R., 2008, MNRAS, 386, 1990
- Micheva G., Iwata I., Inoue A. K., Matsuda Y., Yamada T., Hayashino T., 2015, ArXiv e-prints: 1509.03996
- Miralda-Escude J., Ostriker J. P., 1990, ApJ, 350, 1
- Mitra S., Ferrara A., Choudhury T. R., 2013, MNRAS, 428, L1
- Mitra S., Choudhury T. R., Ferrara A., 2015, MNRAS, 454, L76
- Moretti A., Vattakunnel S., Tozzi P., Salvaterra R., Severgnini P., Fugazza D., Haardt F., Gilli R., 2012, A&A, 548, A87
- Mostardi R. E., Shapley A. E., Steidel C. C., Trainor R. F., Reddy N. A., Siana B., 2015, ApJ, 810, 107
- Nandra K., Pounds K. A., 1994, MNRAS, 268, 405
- Nestor D. B., Shapley A. E., Kornei K. A., Steidel C. C., Siana B., 2013, ApJ, 765, 47
- Noterdaeme P., Ledoux C., Srianand R., Petitjean P., Lopez S., 2009, A&A, 503, 765
- Noterdaeme P. et al., 2012, A&A, 547, L1
- Oesch P. A. et al., 2014, ApJ, 786, 108
- O’Meara J. M., Prochaska J. X., Burles S., Prochter G., Bernstein R. A., Burgess K. M., 2007, ApJ, 656, 666
- O’Meara J. M., Prochaska J. X., Worseck G., Chen H. W., Madau P., 2013, ApJ, 765, 137
- Paardekooper J. P., Pelupessy F. I., Altay G., Kruip C. J. H., 2011, A&A, 530, A87
- Padmanabhan H., Choudhury T. R., Srianand R., 2014, MNRAS, 443, 3761
- Padmanabhan T., 2002, Theoretical Astrophysics - Volume 3, Galaxies and Cosmology
- Palanque-Delabrouille N. et al., 2013, A&A, 551, A29
- Paresce F., McKee C. F., Bowyer S., 1980, ApJ, 240, 387
- Peebles P. J. E., 1993, Principles of Physical Cosmology
- Planck Collaboration et al., 2015, arXiv:1502.01589
- Prochaska J. X., Madau P., O’Meara J. M., Fumagalli M., 2014, MNRAS, 438, 476
- Rahmati A., Pawlik A. H., Raicevic M., Schaye J., 2013, MNRAS, 430, 2427
- Rhoads J. E. et al., 2004, ApJ, 611, 59
- Ricotti M., Shull J. M., 2000, ApJ, 542, 548
- Robertson B. E., Ellis R. S., Furlanetto S. R., Dunlop J. S., 2015, ApJ, 802, L19
- Ross N. P. et al., 2013, ApJ, 773, 14
- Roy A., Nath B. B., Sharma P., 2015, MNRAS, 451, 1939
- Salpeter E. E., 1955, ApJ, 121, 161
- Samui S., Srianand R., Subramanian K., 2007, MNRAS, 377, 285
- Schaye J., 2001, ApJ, 559, 507
- Schenker M. A., Ellis R. S., Konidaris N. P., Stark D. P., 2014, ApJ, 795, 20
- Schulze A., Wisotzki L., Husemann B., 2009, A&A, 507, 781
- Shapiro P. R., Giroux M. L., Babul A., 1994, ApJ, 427, 25
- Shapley A. E., Steidel C. C., Pettini M., Adelberger K. L., Erb D. K., 2006, ApJ, 651, 688
- Shull J. M., Roberts D., Giroux M. L., Penton S. V., Fardal M. A., 1999, aj, 118, 1450
- Shull J. M., Harness A., Trenti M., Smith B. D., 2012, ApJ, 747, 100
- Shull J. M., Moloney J., Danforth C. W., Tilton E. M., 2015, ApJ, 811, 3
- Siana B. et al., 2010, ApJ, 723, 241
- Siana B. et al., 2015, ApJ, 804, 17
- Springel V., 2005, MNRAS, 364, 1105
- Stalin C. S., Petitjean P., Srianand R., Fox A. J., Coppolani F., Schwope A., 2010, MNRAS, 401, 294
- Steidel C. C., Pettini M., Adelberger K. L., 2001, ApJ, 546, 665
- Stevans M. L., Shull J. M., Danforth C. W., Tilton E. M., 2014, ApJ, 794, 75
- Topping M. W., Shull J. M., 2015, ApJ, 800, 97
- Tumlinson J., Giroux M. L., Shull J. M., 2001, ApJ, 550, L1
- Vangioni E., Olive K. A., Prestegard T., Silk J., Petitjean P., Mandic V., 2015, MNRAS, 447, 2575
- Vanzella E. et al., 2010, ApJ, 725, 1011
- Venkatesan A., Giroux M. L., Shull J. M., 2001, ApJ, 563, 1
- Wakker B. P., Hernandez A. K., French D. M., Kim T. S., Oppenheimer B. D., Savage B. D., 2015, ApJ, 814, 40
- Weigel A. K., Schawinski K., Treister E., Urry C. M., Koss M., Trakhtenbrot B., 2015, MNRAS, 448, 3167
- Worseck G., Prochaska J. X., Hennawi J. F., McQuinn M., 2014a, ArXiv e-prints: 1405.7405
- Worseck G. et al., 2014b, MNRAS, 445, 1745
- Wyithe J. S. B., Bolton J. S., 2011, MNRAS, 412, 1926
- Yajima H., Umemura M., Mori M., Nakamoto T., 2009, MNRAS, 398, 715

## APPENDIX A: PHOTOIONIZATION RATES AND CLUMPING FACTOR

In Fig. A1, we show  $\Gamma_{\text{HI}}(z)$  (*thick curves in left-hand panel*) and  $C(z)$  (*right-hand panel*) within the H II bubbles for the models of reionization presented in Section 4.2 and 4.4. For the models of reionization driven by galaxies with constant  $f_{\text{esc}}(z > z_{\text{re}})$  (Section 4.2), the  $\Gamma_{\text{HI}}(z)$  is independent of the  $f_{\text{esc}}$  values in the pre-reionization era. This is an artefact

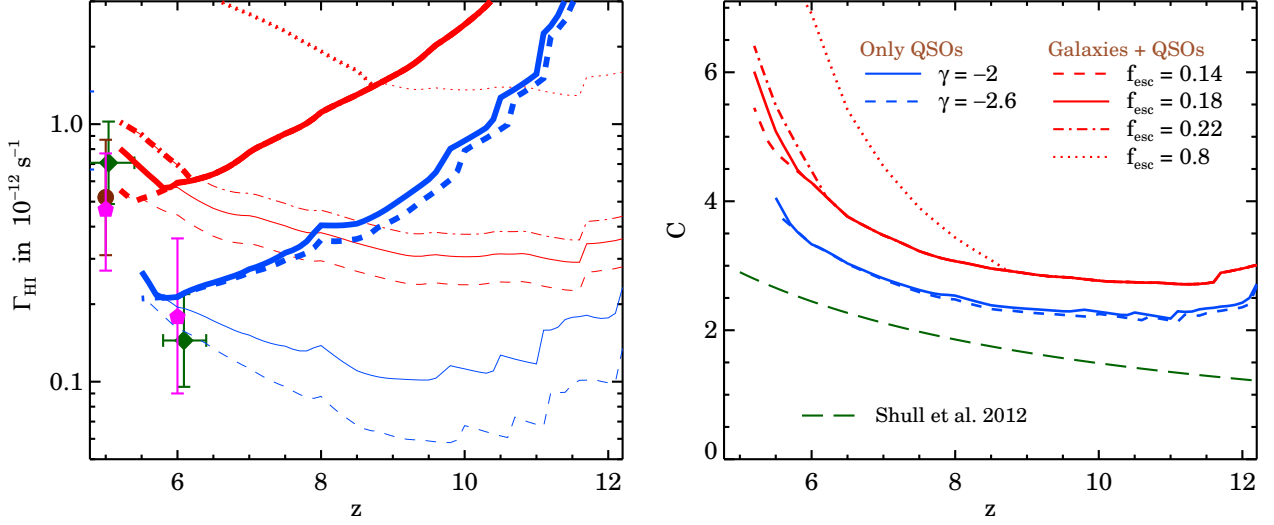


**Figure A1.** *Left:* The mean values of  $\Gamma_{\text{HI}}(z)$  within the H II bubbles (*thick curves*) are shown for different models of reionization discussed in Section 4.2 (Galaxies + QSO models) and Section 4.4 (models with only QSOs). Legends in the *right-hand panel* describe various models. The measurements of  $\Gamma_{\text{HI}}(z)$  are the same as shown in the right-hand panel of Fig. 3. Thin curves represent  $Q_{\text{HII}}(z) \times \Gamma_{\text{HI}}(z)$  which is equivalent to the definition of photoionization rate by HM12. *Right:* The  $C(z)$  is shown corresponding to the  $\Gamma_{\text{HI}}(z)$  within the H II bubbles (as shown in the *left-hand panel*). For comparison, we also show the mean value of  $C(z)$  obtained by Shull et al. (2012).

of using constant  $f_{\text{esc}}(z > z_{\text{re}})$ . Under this assumption, the  $Q_{\text{HII}}$  at any  $z$  in pre-reionization era scales with the value of  $f_{\text{esc}}$ , as evident from Eq. (10). In the same way, the  $J_{\nu}$  scales with the  $f_{\text{esc}}/Q_{\text{HII}}(z)$ . Therefore, the  $\Gamma_{\text{HI}}(z)$  becomes independent of the  $f_{\text{esc}}$  in the pre-reionization era.

The  $\Gamma_{\text{HI}}(z)$  values for models of reionization driven by galaxies are consistent with the measurements at  $z \sim 5$  but off by 1 to 2- $\sigma$  level at  $z \sim 6$ .  $\Gamma_{\text{HI}}(z)$  for the models of reionization by QSOs alone (Section 4.4) are consistent with the measurements at  $z \sim 6$ . Main reason for this difference in  $\Gamma_{\text{HI}}(z)$  in the galaxy dominated and QSO dominated models of reionization is arising because of the different SEDs of the galaxies and QSOs. The SED for QSOs (with  $\alpha = -1.4$ ) is more flat than the SED of galaxies ( $\beta = -1.8$ ). Therefore, to obtain the same  $\dot{n}$ , galaxies need more photons at H I ionizing edge as compared to QSOs. This eventually leads to a higher  $\Gamma_{\text{HI}}$ , due to the  $\nu^{-3}$  dependence of  $\sigma_{\text{HI}}(\nu)$ , in the models where galaxies dominate the reionization. In the *left-hand panel* of Fig. A1 we also show the  $Q_{\text{HII}}(z) \times \Gamma_{\text{HI}}(z)$  (*thin curves*), that is equivalent to the definition of photoionization rate by HM12.

The corresponding  $C(z)$ , shown in the *right-hand panel* of Fig. A1, is calculated in the simulation box at different  $z$ . It is then extrapolated at  $z$  where we do not have the stored simulation boxes. The  $C(z)$  depends on the  $\Gamma_{\text{HI}}(z)$  within the H II bubbles. Therefore, for galaxy dominated reionization models,  $C(z)$  is independent of the values of  $f_{\text{esc}}$  in the pre-reionization era. For comparison, we also show the mean value of  $C(z)$  obtained by Shull et al. (2012) which is systematically lower than what we obtain for both cases.